ATLAS CONF Note

ATLAS-CONF-2017-072

September 19, 2017

Prompt photon production in $\sqrt{s_{\mathrm{NN}}} = 8.16$ TeV p+Pb collisions with ATLAS

The ATLAS Collaboration

The inclusive production cross-section for isolated, prompt photons in p+Pb collisions at $\sqrt{s_{\mathrm{NN}}} = 8.16$ TeV is studied with the ATLAS detector at the LHC using a data set with an integrated luminosity of 162 nb^{-1}. The cross-section is measured as a function of photon transverse energy from 25 to 500 GeV and over nearly five units of pseudorapidity, including kinematic regions in both the downstream proton– and nucleus–going directions. Results are reported in the nucleon–nucleon center of mass collision frame. The nuclear modification factor $R_{p\mathrm{Pb}}$ is reported using a extrapolation, derived using NLO pQCD, of a previous measurement of photon production in pp collisions at 8 TeV. The cross-sections and $R_{p\mathrm{Pb}}$ values are compared to the results of a next-to-leading order perturbative QCD calculation and to the expectations based on a picture of the energy loss of partons incoming to the hard scattering. At large nucleus-going rapidity, the cross-section is suppressed due to the different up and down valence quark content of the nucleus relative to that of the proton. The data are consistent with global analyses of the parton densities in nuclei, and disfavor a large amount of energy loss in the initial state.

ATLAS-CONF-2017-072
25 September 2017

1 Introduction

Measurements of photon production rates at large transverse energy (E_{T}^{γ}) are a fundamental way to characterize a hadronic collision system. In collisions involving large nuclei, such measurements are a potentially sensitive probe of how parton densities are modified in a nuclear environment [1–3]. Additionally, while photon production rates are not expected to be modified through interactions in the final state with the hot nuclear medium formed in nucleus–nucleus collisions, they may be changed due to an energy loss arising through interactions in the initial stages of the collision [4, 5]. Constraints on such initial state effects are particularly important for putting into context the observed modifications of strongly interacting processes, such as jet and hadron production [6, 7], since they are sensitive to both initial- and final-state effects. In proton–nucleus collisions, such measurements can be performed with better systematic control, and over a broader kinematic range, than in nucleus–nucleus collisions, allowing for a more precise constraint on these initial state effects.

Prompt photon production processes have been extensively measured in proton–proton (pp) collisions at a variety of collision energies [8–12] at the Large Hadron Collider (LHC). They have also been measured in lead–lead (Pb+Pb) collisions at $\sqrt{s_{\mathrm{NN}}} = 2.76$ TeV [13, 14], where the data indicate that photon production rates are unaffected from the passage of the photons through the hot nuclear medium. At the Relativistic Heavy Ion Collider, photon production rates have been measured in deuteron–gold collisions at $\sqrt{s_{\mathrm{NN}}} = 200$ GeV [15, 16], constraining the possible amount of energy loss in the inital state.

Previous measurements in 28 nb^{-1} of proton–lead (p+Pb) collision data at $\sqrt{s_{\mathrm{NN}}} = 5.02$ TeV have been made for final states which are strongly interacting, such as jet production [17], and those which are not, such as Z boson production [18], which have provided some constraints on initial-state effects. This note reports a measurement of the isolated, prompt photon production cross-section over a broad kinematic range in p+Pb collisions at $\sqrt{s_{\mathrm{NN}}} = 8.16$ TeV. Therefore, this measurement offers a probe of these effects through a more abundant channel and in a data set with more than five times the integrated luminosity relative to that at 5.02 TeV.

The data used in this analysis were collected with the ATLAS detector during the p+Pb collision running period of 2016, corresponding to an integrated luminosity of 162 nb^{-1}. The proton and lead beams were respectively configured with an energy of 6.5 TeV and $Z \times 6.5$ TeV, where $Z = 82$ is the atomic number. In the lead nucleus, the energy per nucleon was therefore $(Z/A) \times 6.5$ TeV, where $A = 208$ is the nuclear mass number, resulting in a nucleon–nucleon center of mass collision energy of 8.16 TeV and a rapidity boost of this frame by ± 0.465 units relative to the ATLAS laboratory frame[1]. Data taking was divided into two periods with different configurations of the LHC beams. In the first period, the lead ions circulated in beam 1 (clockwise, towards negative rapidity) and protons circulated in beam 2, while in the second period they were reversed. These corresponded to 56 nb^{-1} and 106 nb^{-1} respectively. By convention, the results are reported as a function of photon pseudorapidity in the nucleon–nucleon collision frame, η^{*}, with a positive (negative) pseudorapidity corresponding to photon production in the forward or downstream proton (backward or downstream nuclear) beam direction.

In a leading order picture, $p + \mathrm{Pb} \rightarrow \gamma + X$ has contributions from direct processes, in which the photon is produced in the hard interaction, and fragmentation processes, in which it is produced in

[1] ATLAS uses a right-handed coordinate system with its origin at the nominal interaction point (IP) in the centre of the detector and the z-axis along the beam pipe. The x-axis points from the IP to the centre of the LHC ring, and the y-axis points upward. Cylindrical coordinates (r, ϕ) are used in the transverse plane, ϕ being the azimuthal angle around the z-axis. The pseudorapidity is defined in terms of the polar angle θ as $\eta = -\ln\tan(\theta/2)$.

the parton shower. Beyond leading order the direct and fragmentation components have no physical meaning and cannot be factorized; the sum of their cross sections is the physical observable. However, the impact of the fragmentation contribution can be reduced through the use of isolation criterion, which also suppresses the background associated to photons issued from the decays of neutral hadrons in jets. The measurements presented in this note correspond to an isolation prescription, used in previous measurements by ATLAS [9], in which the transverse energy sum within a $\Delta R = \sqrt{(\Delta\eta)^2 + (\Delta\phi)^2} < 0.4$ cone around the photon, $E_{\mathrm{T}}^{\mathrm{iso}}$, is required to be smaller than $4.8\ \mathrm{GeV} + 4.2 \times 10^{-3} E_{\mathrm{T}}^{\gamma}[\mathrm{GeV}]$. At the generator level, all final-state particles excluding muons and neutrinos are included in the sum.

The measurements are compared to next-to-leading-order (NLO) QCD predictions from JETPHOX [19], which incorporate the free nucleon parton distribution functions (PDFs) and also the nuclear modifications to these extracted from global analyses [20, 21]. Additionally, the nuclear modification factor $R_{p\mathrm{Pb}}$ is reported in each pseudorapidity selection as a function of E_{T}^{γ}. The $R_{p\mathrm{Pb}}$ is defined as the ratio of the cross-section in p+Pb collisions to A times the cross-section in pp collisions at the same $\sqrt{s}$,

$$R_{p\mathrm{Pb}} = (d\sigma^{p+\mathrm{Pb}\to\gamma+X}/dE_{\mathrm{T}}^{\gamma})/(A \cdot d\sigma^{pp\to\gamma+X}/dE_{\mathrm{T}}^{\gamma}) \tag{1}$$

For this purpose, a previous measurement of prompt photon production in pp collisions at $\sqrt{s} = 8$ TeV [9], is used to form the reference data. Since the up and down quark content of the proton is different than that of the lead nucleus, in the kinematic region dominated by production from the nuclear valence region (large E_{T}^{γ}, negative η^{γ}), the $R_{p\mathrm{Pb}}$ is expected to deviate from unity even in the absence of any additional nuclear effects.

2 Experimental setup

The ATLAS detector [22] is a multi-purpose detector with a forward-backward symmetric cylindrical geometry. For this measurement, its relevant components include an inner tracking detector surrounded by a thin superconducting solenoid, electromagnetic and hadronic calorimeters, and a high-level online trigger system. The inner-detector system is immersed in a 2 T axial magnetic field and provides charged-particle tracking in the range $|\eta| < 2.5$. In order of closest to furthest from the beam pipe, it consists of a high-granularity silicon pixel detector, a silicon microstrip tracker, and the transition radiation tracker. The calorimeter system covers the range $|\eta| < 4.9$. In the region $|\eta| < 3.2$, electromagnetic calorimetry is provided by barrel and endcap high-granularity lead/liquid-argon (LAr) electromagnetic calorimeters, with an additional thin LAr presampler covering $|\eta| < 1.8$ to correct for energy loss in material upstream of the calorimeters. Within the region of the measurement, the LAr calorimeters are divided into three layers in depth. Hadronic calorimetry is provided by a steel/scintillator-tile calorimeter, segmented into three barrel structures within $|\eta| < 1.7$, and two copper/LAr hadronic endcap calorimeters, which cover the region $1.5 < |\eta| < 3.2$. Finally, the forward hadronic calorimeter covers $3.1 < |\eta| < 4.9$ in the lab frame.

During data-taking events are initially selected using a first-level trigger based on energy deposition in the electromagnetic calorimeter implemented in custom electronics. Software algorithms with access to the full detector information are then used in the high-level trigger [23] to select events consistent with a high-E_{T}^{γ} photon candidate. The high-level triggers used in this analysis were configured with four online E_{T}^{γ} thresholds from 20 to 35 GeV. The highest-threshold trigger sampled the full luminosity and is

used over most of the kinematic range in the measurement, while the lower-threshold triggers are used to perform the measurement at low-E_{T}^{γ}.

Photons are reconstructed following a procedure used extensively in previous ATLAS measurements (for example in $\sqrt{s}$ = 13 TeV collision data recorded in 2015 [10]), of which only the main features are summarized here. In the laboratory frame, photon pseudorapidity, η^{γ}, is measured in the range $|\eta^{\gamma}| < 2.37$, but excluding the transition region between the barrel and endcap calorimeters which subtends $1.37 < |\eta^{\gamma}| < 1.56$.

Photon candidates are reconstructed from clusters of energy deposited in the electromagnetic calorimeter and classified as unconverted or converted photons based on the presence or absence of a matching reconstructed track or conversion vertex. The photon identification is based on shower shapes in the calorimeter (the *tight* cuts described in Ref. [24]), selecting those which are compatible with that originating from a single photon impacting the calorimeter. These include information from the hadronic calorimeter, the lateral shower shape in the second layer of the electromagnetic calorimeter, and the detailed shower shape in the finely-segmented first layer, and the photon identification criteria are applied separately for converted and unconverted photons.

The measurement of the photon energy is based on the energy collected in calorimeter cells in an area of size $\Delta\eta \times \Delta\phi = 0.075 \times 0.175$ in the barrel and $\Delta\eta \times \Delta\phi = 0.125 \times 0.125$ in the end-caps. It is corrected via a dedicated energy calibration [25] which accounts for upstream losses, both lateral and longitudinal leakage, and for the sampling fraction variation with energy and shower depth. The isolation transverse energy, $E_{\mathrm{T}}^{\mathrm{iso}}$, is computed from the E_{T} sum of topological clusters of calorimeter cells [26] inside a cone size of $R = 0.4$ centered on the photon. This cone size is chosen to be compatible with a previous measurement of photon production in pp collisions at $\sqrt{s}$ = 8 TeV [9], which is used to construct the reference spectrum for the $R_{p\mathrm{Pb}}$ measurement, and since it is a value for which next-to-leading calculations have been shown to be reliable. This estimate excludes a small area centered on the photon, and is corrected for the expected leakage of the photon energy from this region into the isolation cone. Unlike what was done in [9], this analysis performs no jet area subtraction on $E_{\mathrm{T}}^{\mathrm{iso}}$ at either reconstructed or generator levels.

3 Monte Carlo and theoretical predictions

Samples of Monte Carlo (MC) events are generated to study the performance for signal photons. The Pythia 8.186 [27] generator was used with the NNPDF23LO PDF set [28], and a set of generator parameters tuned to reproduce a set of minimum-bias data ("A14" tune) [29]. The generator simulates the direct photon contribution and, through final-state QED radiation in $2 \rightarrow 2$ QCD processes, also includes the fragmentation photon contributions. Six million total events were generated, corresponding to six exclusive selections on the final state photon E_{T}^{γ}. Events were passed through a full GEANT4 simulation of the ATLAS detector [30, 31], and were digitized and reconstructed in the same way as the data. The simulated events were overlaid with minimum-bias p+Pb data events, which were split between the two beam configurations in a way equivalent to that in data-taking, and a distribution of event activity values corresponding to that present in photon-containing events in data. In this way, the MC events contain the effects of the p+Pb underlying event identical to that observed in data. In MC samples, the resulting photon shower shapes and extracted identification efficiency are adjusted for small differences previously observed between these quantities in data and simulation [24].

The fiducial definition of the measurement corresponds to photons with $E_{\mathrm{T}}^{\gamma} > 25$ GeV and isolation energy $E_{\mathrm{T}}^{iso} < 4.8\ \mathrm{GeV} + 4.2 \times 10^{-3} E_{\mathrm{T}}^{\gamma}[\mathrm{GeV}]$ consistent with previous measurements [9, 10] as described above, and in the laboratory frame pseudorapidity selections detailed above. The data in this note are compared to an NLO pQCD prediction which includes free nucleon and nuclear PDFs, and to an initial state energy loss model, which are described below.

The pQCD prediction is similar to that used in Ref. [3], but using the updated PDF set CT14 [33]. Jetphox [19] is used to perform a full NLO pQCD calculation of the direct and fragmentation contributions to the cross-section. The BFG set II [32] of parton–to–photon fragmentation functions and the CT14 PDF set for the free nucleon parton densities are used, the number of massless quark flavors is set to five, and the renormalization, factorization and fragmentation scales are chosen to be E_{T}^{γ}. In addition to the calculation with the free nucleon PDFs, separate calculations incorporating the EPPS16 [20] and nCTEQ15 [21] nuclear PDF sets are performed. The EPPS16 calculation uses the same free proton PDF set, CT14, as its baseline. For the calculation of the cross-section, a coherent factor of two variation of the three scales above, as well as the nuclear PDF error sets, are used to estimate the theoretical systematic uncertainty. For the calculation of the $R_{p\mathrm{Pb}}$, only the nPDF uncertainties are considered since previous calculations have shown that the scale uncertainties cancel efficiently in the kinematic region of the measurement [3]. No non-perturbative corrections are applied to Jetphox for this analysis.

The initial state energy loss calculation is performed within the framework described in Refs. [4, 5, 34]. In this picture, the energetic partons undergo multiple scattering in the cold nuclear medium, and thus lose energy due to this medium-induced gluon bremsstrahlung, before the hard collision. The calculation is performed with a parton–gluon momentum transfer $\mu = 0.35$ GeV and mean free path for quarks $\lambda_q = 1.5$ fm. Alternate calculations with a shorter path length ($\lambda_q = 1$ fm), and a control version with no initial state energy loss, is also performed.

4 Data analysis

The differential cross-section is constructed as follows,

$$d\sigma/dE_{\mathrm{T}}^{\gamma} = \frac{1}{L_{\mathrm{int}}} \frac{1}{\Delta E_{\mathrm{T}}^{\gamma}} \frac{N_{\mathrm{sig}} P_{\mathrm{sig}}}{\epsilon^{\mathrm{sel}} \epsilon^{\mathrm{trig}}} C, \tag{2}$$

where L_{int} is the integrated luminosity, N_{sig} is the yield of photon candidates passing identification and isolation requirements, P_{sig} is the purity of signal photons in this selection, ϵ^{sel} is the combined reconstruction, identification and isolation efficiency for signal photons, ϵ^{trig} is the trigger efficiency, and C is a correction for the bin migration in E_{T}^{γ} caused by detector inefficiencies and the finite resolution of the photon energy measurement. In general, the sizes of the corrections which enter Eq. 2 are similar to those in the analysis of $\sqrt{s} = 13$ TeV pp data recorded in the same year [10].

The purity P_{sig} is determined via a double sideband procedure used extensively in previous measurements of cross-sections with a photon in the final state [9, 10, 35, 36]. In the procedure, four sideband regions are defined, corresponding to the categorization of photons along two axes: (1) the isolation axis, corresponding to isolated and an inverted "non-isolated" selection, (2) the identification axis, corresponding to photons that pass the identification requirements above, and those that pass an inverted requirement designed to select predominantly background. The majority of signal photons are in the identified, isolated

region, while the other regions are dominated by the background. Photon candidates that comprise the background are assumed to be distributed in a way that is uncorrelated along the two axes. The yield in the three non-signal sidebands can be used to extract the purity in the signal sideband. The procedure also accounts for the small fraction of signal photons which are reconstructed in the non-signal sidebands, quantities, known as leakage fractions, determined from simulation samples. The purity is typically 60% at the $E_{\mathrm{T}}^{\gamma} = 25$ GeV, rises to 80% at $E_{\mathrm{T}}^{\gamma} = 100$ GeV and asymptotically approaches unity, reaching 99% at $E_{\mathrm{T}}^{\gamma} = 300$ GeV.

The combined selection efficiency for signal photons, ϵ^{sel}, is determined in simulation and is typically 90% at all E_{T}^{γ} and η^{γ}, except at the lowest E_{T}^{γ} where it decreases to 85%. Trigger efficiencies ϵ^{trig} are studied using events selected with minimum-bias triggers, Level-1 triggers without additional requirements, and high level photon triggers without identification requirement. For each kinematic selection in the measurement, the yield is constructed using the highest-luminosity trigger for which the kinematic region is on its efficiency plateau, which was determined to be greater than 99% for all triggers. No correction is applied for any residual trigger inefficiency.

In MC events, the energy response for identified, isolated photons, defined as the ratio of the reconstructed to true energy, is found to be within 1% of unity, with a resolution that decreases from 3% to 2% over the E_{T}^{γ} range of the measurement. The bin migration correction factors C are defined in simulation as the ratio of the photon spectrum where the E_{T}^{γ} is evaluated at the reconstructed level, to that with the E_{T}^{γ} at the generator level. These are typically within 2–3% of unity, and within 5% of unity at the largest E_{T}^{γ} values.

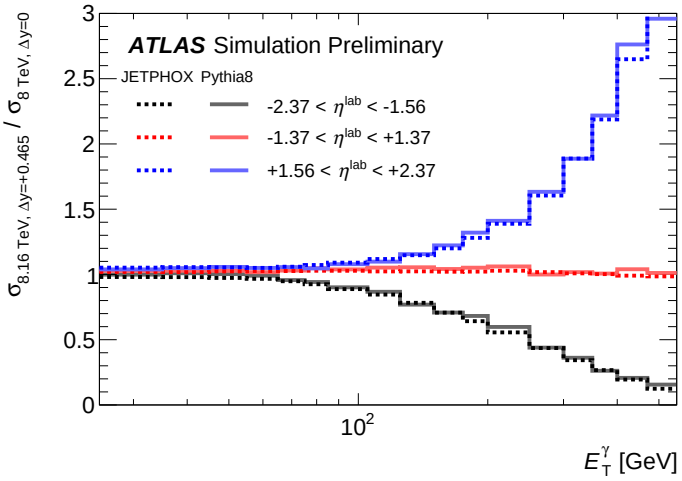

Figure 1: Summary of extrapolation factors applied to the measured pp $\sqrt{s} = 8$ TeV data to construct an approximate $\sqrt{s} = 8.16$ TeV spectrum matching the shift of the center of mass in p+Pb data plotted as a function of generator level photon transverse energy. The factors determined using JETPHOX (dashed lines) and Pythia8 (solid lines) are shown for the three η^{lab} ranges used in the analysis (different colors).

To construct an appropriate pp spectrum which matches the collision energy and center of mass frame of the p+Pb system, simulation is used to extrapolate the previously measured $\sqrt{s} = 8$ TeV pp data by ATLAS [9]. For each kinematic selection, the ratio of a JETPHOX calculation for pp collisions at 8.16 TeV with a boost of the center of mass corresponding to the p+Pb system, to that in 8 TeV pp is determined for each η^{lab} selection. These factors are shown in Fig. 1 and are applied as multiplicative factors to

the measured 8 TeV data, and primarily correct for the boost of the p+Pb system. At mid-rapidity, or at low-$E_{\mathrm{T}}^{\gamma} < 100$ GeV at large rapidities, the factors are typically within a few percent of unity. However, at large E_{T}^{γ}, where the rapidity distribution becomes steeper, the extrapolation factors become much more sensitive to the rapidity shift from the center of mass boost between the frames, and at large pseudorapidity, they reach up to a factor of 2–3. An alternate set of factors, derived from the generator-level predictions of Pythia8, is also shown in Fig. 1 and are used to assess the sensitivity of the extrapolation factors to the physics model.

5 Systematic uncertainties

The primary sources of systematic uncertainties affecting the measurement are investigated. These include uncertainties related to the selection and purity of photons, to the photon energy scale and resolution, a residual contribution of isolated electrons to the measurement, the reference pp spectra and the extrapolation to the kinematics of the measurement, and the luminosity of the data sample.

The sensitivity of the measurement to the photon selection, identification and purity determination is tested in several ways: the reconstructed level isolation definition is varied to check that the resulting change in the yield is offset by the change in signal photon purity; the inverted isolation requirement is varied to select a different set of background candidates; the inverted identification requirement is varied to select a variety of samples that would completely represent the properties of the background events in the signal region; a degree of correlation of the background along the isolation and identification axes is considered; and the uncertainty on the efficiency in simulation is accounted. Additionally, the uncertainty in the extracted purity from limited statistics in the sideband regions is propagated as a statistical uncertainty in the measurement. As previous results [10] suggest that the model dependence of the truth isolation definition is negligible compared to the other isolation uncertainties, it is not considered here. The total uncertainty from this category, which is codominated by the uncertainty associated with sideband background correlation and the non-tight definition, a selection in shower shapes meant to enhance backgrounds, is 10% at the lowest E_{T}^{γ} value and is systematically smaller with increasing E_{T}^{γ}.

A detailed description of the several components of the photon energy scale and resolution uncertainties are given in Ref. [10]. The impact of these on the measurement is determined by varying the reconstructed photon E_{T}^{γ} in simulation and deriving alternate correction factors. In this analysis, a single overall variation is used according to the quadrature sum of the energy scale and, separately, resolution uncertainties. The resulting energy scale uncertainties are dominant and range from a few percent at low-E_{T}^{γ} and mid-rapidity to 5–10% at large E_{T}^{γ} and/or large pseudorapidity.

The relative mixture of direct and fragmentation photons in a given E_{T}^{γ} slice is model dependent and affects both the estimation of photon purity through leakage fractions, and the overall efficiency. A detailed study of the sensitivity of the photon cross section to changes in this mixture in 8 TeV pp was completed in [9]. For this note, the same sensitivity is assumed and the uncertainty associated to this mixture from [9] is added in quadrature with the rest of the systematic uncertainty on the cross section.

An uncertainty is assigned to cover the possible contribution of mis-reconstructed electrons, primarily from the decays of $W^{\pm}$ and Z bosons in the electron channel, to the selected photon yield. Based on the results of previous analyses with the identical detector and reconstruction setup [9, 10], this is conservatively assigned to be 1% for $E_{\mathrm{T}}^{\gamma} < 105$ GeV, above which it is negligible.

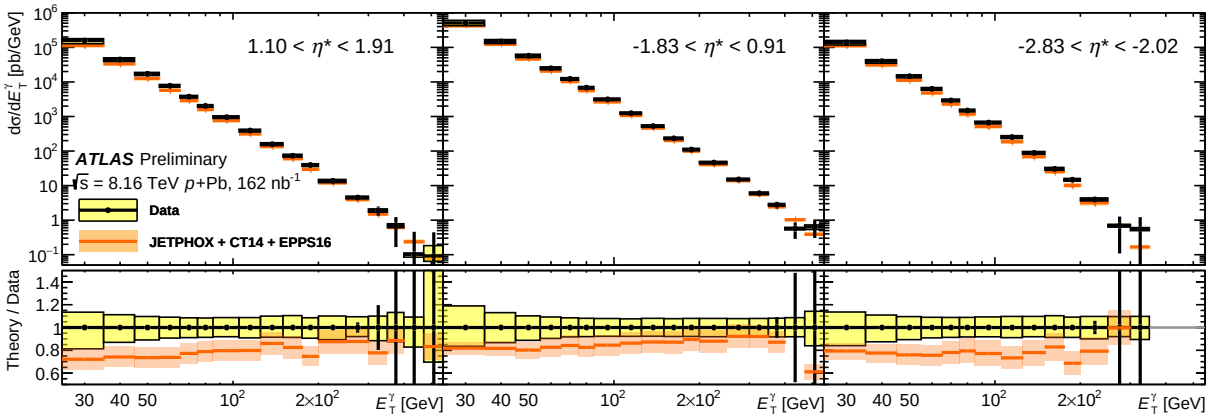

Figure 2: Isolated, prompt photon cross-sections as a function of E_{T}^{γ}, shown for different η^{*} selections in each panel. The data are compared to JETPHOX with the EPPS16 nuclear PDF set, with the theory to data ratio shown in lower panels. Yellow bands correspond to total systematic uncertainties on the data, vertical bars correspond to the statistical uncertainties on the data, and the orange bands correspond to the uncertainties on the theoretical calculation (see text).

The uncertainty on the pp reference is obtained directly from that reported in the measurement [9], with the conservative assumption that they are completely uncorrelated with the uncertainties in the measurement in the p+Pb system. The uncertainty on the extrapolation of this spectrum is determined by using an alternate method to derive the multiplicative extrapolation factors. Instead of JETPHOX, the central values of the generator-level cross-section in Pythia8 for the rapidity-boosted $\sqrt{s} = 8.16$ TeV and 8 TeV kinematics are used. The difference in the extrapolation factors, which is at most a few percent in the kinematic region of the measurement, is used as an estimate of the uncertainty in the extrapolation procedure.

Finally, a global uncertainty on the luminosity of 6.2% is derived through an analysis of beam separation scans similar to that in Ref. [37], and is fully correlated between all kinematic selections.

6 Results

Photon production cross-sections are reported for photons with $E_{\mathrm{T}}^{\gamma} > 25$ GeV in the following pseudorapidity selections in the nucleon–nucleon frame: $-2.83 < \eta^{*} < -2.02$, $-1.83 < \eta^{*} < 0.91$ and $1.10 < \eta^{*} < 1.91$. These correspond to the acceptance of the ATLAS detector in the laboratory frame of $|\eta^{\gamma}| < 1.37$ and $1.56 < |\eta^{\gamma}| < 2.37$. Photons are required to be isolated according to $E_{\mathrm{T}}^{\mathrm{iso}} < 4.8\ \mathrm{GeV} + 4.2 \times 10^{-3} E_{\mathrm{T}}^{\gamma}[\mathrm{GeV}]$,

Figure 2 shows the prompt, isolated photon cross-section as functions of E_{T}^{γ} and η^{*}. The measured $d\sigma/dE_{\mathrm{T}}^{\gamma}$ decreases by five orders of magnitude over the complete E_{T}^{γ} range, with an observed yield for $E_{\mathrm{T}}^{\gamma} \approx 500$ GeV photons at mid-rapidity. The experimental uncertainties range from 10% at low and high E_{T}^{γ}, where they are dominated by the purity and energy scale uncertainties respectively, but reach a minimum of $\approx 6\%$ at $E_{\mathrm{T}}^{\gamma} \approx 100$ GeV, where both of these sources are modest. The JETPHOX calculation systematically underpredicts the data by up to 20% at low E_{T}^{γ} but gets asymptotically closer to the data at higher E_{T}^{γ}, consistent with the results of such comparisons in pp collisions at similar energies [9, 10].

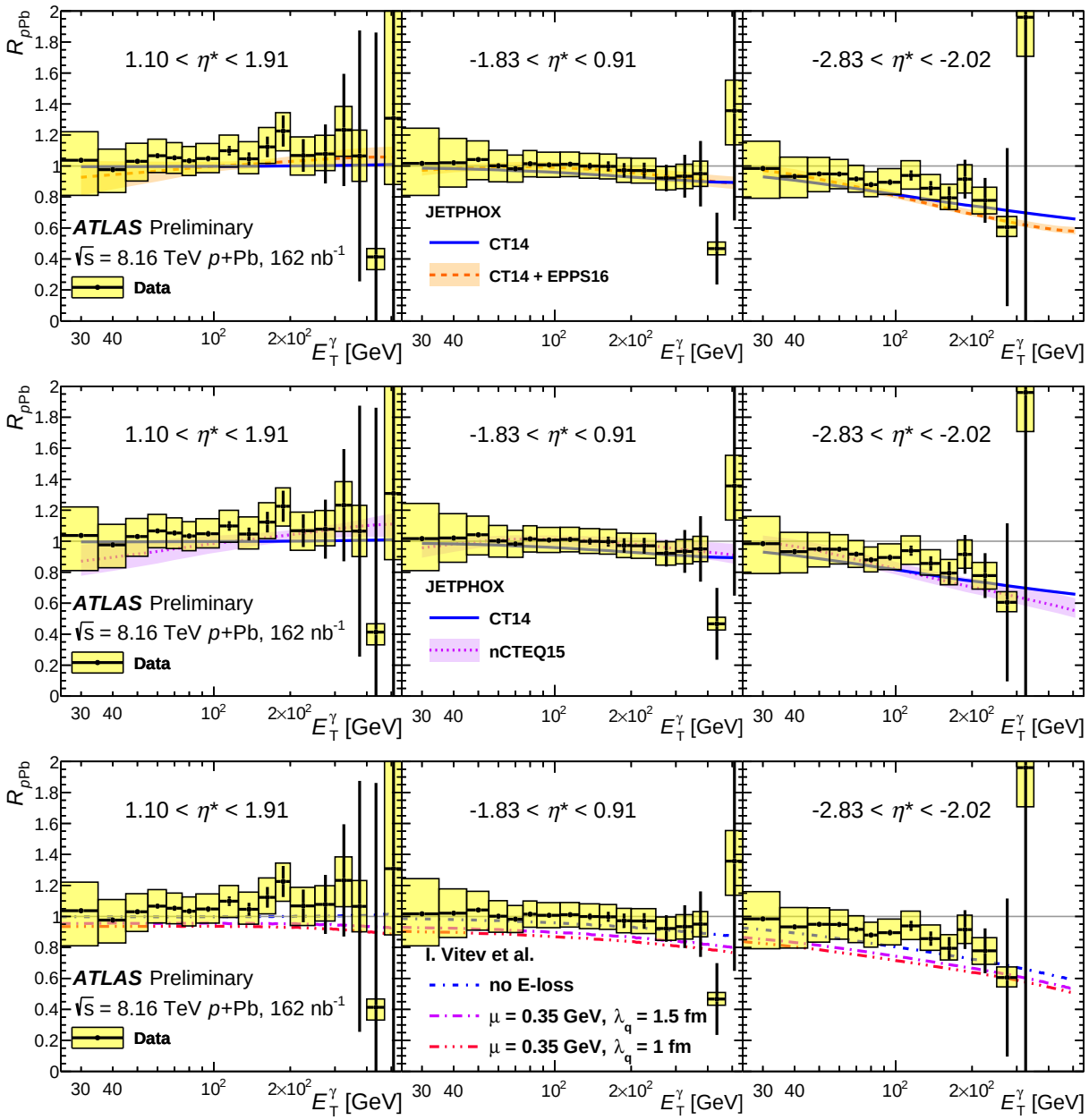

Figure 3: Nuclear modification factor $R_{p\mathrm{Pb}}$ for isolated, prompt photons as a function of E_{T}^{γ}, shown for different η^* selections in each panel. The data are identical in each row, but show comparisons to the expectations based on JETPHOX with the EPPS16 nuclear PDF set (top) or with the nCTEQ15 nuclear PDF set (middle), and with an initial state energy loss calculation (bottom). In all plots, the yellow bands and vertical bars correspond to total systematic and statistical uncertainties on the data, respectively. In the top and middle panels, the orange and purple bands correspond to the systematic uncertainties on the calculations (see text).

Figure 3 shows the nuclear modification factor $R_{p\mathrm{Pb}}$ as functions of E_{T}^{γ} and η^{*}. At forward rapidities and low to moderate E_{T}^{γ} at mid-rapidity, the $R_{p\mathrm{Pb}}$ is consistent with unity, indicating that isospin or other nuclear effects are small. At high E_{T}^{γ} and backward pseudorapidity, the $R_{p\mathrm{Pb}}$ is significantly lower than unity. This feature primarily reflects the difference in the up and down quark composition of the nucleus relative to the proton, for which the larger relative down quark density decreases the matrix element for diagrams with an outgoing photon. This effect is evident in the JETPHOX theory curve in blue which includes the proton-neutron asymmetry and the free proton PDF set CT14. Within the present uncertainties, the central values of the data are consistent with both the free proton PDFs and with the small effects expected from a nuclear modification of the parton densities. However, the data do disfavor a large suppression in the cross-section due to energy loss effects.

7 Conclusion

This note presents a measurement of the inclusive prompt photon cross-section in p+Pb collisions at $\sqrt{s_{\mathrm{NN}}} = 8.16$ TeV. The cross-section is reported in three pseudorapidity selections with respect to the nucleon–nucleon collision frame, and covers the kinematic region $E_{\mathrm{T}}^{\gamma} = 25$–$500$ GeV. The data are compared to a next-to-leading order calculation which incorporates nuclear PDF effects. A measurement of the nuclear modification factor, R_{pPb}, is reported using a NLO pQCD-based extrapolation of previously published pp data at $\sqrt{s} = 8$ TeV. The data are compatible with the modest degree to which PDFs are expected to be modified in nuclei in this kinematic region and may help to place an upper limit on the possible amount of energy lost by hard partons in the initial stages of nuclear collisions.

References

[1] Salgado et al., *Proton-Nucleus Collisions at the LHC: Scientific Opportunities and Requirements*, J. Phys. **G39** (2012) p. 015010, arXiv: 1105.3919 [hep-ph].

[2] Arleo, Eskola, Paukkunen, and Salgado, *Inclusive prompt photon production in nuclear collisions at RHIC and LHC*, JHEP **04** (2011) p. 055, arXiv: 1103.1471 [hep-ph].

[3] Helenius, Eskola, and Paukkunen, *Probing the small-x nuclear gluon distributions with isolated photons at forward rapidities in p+Pb collisions at the LHC*, JHEP **09** (2014) p. 138, arXiv: 1406.1689 [hep-ph].

[4] Vitev and Zhang, *A Systematic study of direct photon production in heavy ion collisions*, Phys. Lett. **B669** (2008) p. 337, arXiv: 0804.3805 [hep-ph].

[5] Kang, Vitev, and Xing, *Effects of cold nuclear matter energy loss on inclusive jet production in p+A collisions at energies available at the BNL Relativistic Heavy Ion Collider and the CERN Large Hadron Collider*, Phys. Rev. **C92** (2015) p. 054911, arXiv: 1507.05987 [hep-ph].

[6] ATLAS Collaboration, *Measurements of the Nuclear Modification Factor for Jets in Pb+Pb Collisions at* $\sqrt{s_{\mathrm{NN}}} = 2.76$ *TeV with the ATLAS Detector*, Phys. Rev. Lett. **114** (2015) p. 072302, arXiv: 1411.2357 [hep-ex].

[7] ATLAS Collaboration, *Measurement of charged-particle spectra in Pb+Pb collisions at* $\sqrt{s_{\mathrm{NN}}} = 2.76$ *TeV with the ATLAS detector at the LHC*, JHEP **09** (2015) p. 050, arXiv: 1504.04337 [hep-ex].

[8] ATLAS Collaboration, *Measurement of the inclusive isolated prompt photon cross section in pp collisions at* $\sqrt{s} = 7$ *TeV with the ATLAS detector*, Phys. Rev. D **83** (2011) p. 052005, arXiv: 1012.4389 [hep-ex].

[9] ATLAS Collaboration, *Measurement of the inclusive isolated prompt photon cross section in pp collisions at* $\sqrt{s} = 8$ *TeV with the ATLAS detector*, JHEP **08** (2016) p. 005, arXiv: 1605.03495 [hep-ex].

[10] ATLAS Collaboration, *Measurement of the cross section for inclusive isolated-photon production in pp collisions at* $\sqrt{s} = 13$ *TeV using the ATLAS detector*, Phys. Lett. B **770** (2017) p. 473, arXiv: 1701.06882 [hep-ex].

[11] CMS Collaboration, *Measurement of the Differential Cross Section for Isolated Prompt Photon Production in pp Collisions at* 7 *TeV*, Phys. Rev. D **84** (2011) p. 052011, arXiv: 1108.2044 [hep-ex].

[12] CMS Collaboration, *Measurement of the Production Cross Section for Pairs of Isolated Photons in pp collisions at* $\sqrt{s} = 7$ *TeV*, JHEP **01** (2012) p. 133, arXiv: 1110.6461 [hep-ex].

[13] ATLAS Collaboration, *Centrality, rapidity and transverse momentum dependence of isolated prompt photon production in lead–lead collisions at* $\sqrt{s_{\mathrm{NN}}} = 2.76$ *TeV measured with the ATLAS detector*, Phys. Rev. C **93** (2016) p. 034914, arXiv: 1506.08552 [hep-ex].

[14] ALICE Collaboration, *Direct photon production in Pb-Pb collisions at* $\sqrt{s_{\mathrm{NN}}} = 2.76$ *TeV*, Phys. Lett. **B754** (2016) p. 235, arXiv: 1509.07324 [nucl-ex].

[15] STAR Collaboration, *Inclusive* π^0*,* η*, and direct photon production at high transverse momentum in p + p and d+Au collisions at* $\sqrt{s_{NN}} = 200$ *GeV*, Phys. Rev. **C81** (2010) p. 064904, arXiv: 0912.3838 [hep-ex].

[16] PHENIX Collaboration, *Direct photon production in d+Au collisions at* $\sqrt{s_{NN}} = 200$ *GeV*, Phys. Rev. **C87** (2013) p. 054907, arXiv: 1208.1234 [nucl-ex].

[17] ATLAS Collaboration, *Centrality and rapidity dependence of inclusive jet production in* $\sqrt{s_{\mathrm{NN}}} = 5.02$ *TeV proton-lead collisions with the ATLAS detector*, Phys. Lett. B **748** (2015) p. 392, arXiv: 1412.4092 [hep-ex].

[18] ATLAS Collaboration, *Z boson production in p + Pb collisions at* $\sqrt{s_{\mathrm{NN}}} = 5.02$ *TeV measured with the ATLAS detector*, Phys. Rev. C **92** (2015) p. 044915, arXiv: 1507.06232 [hep-ex].

[19] Aurenche, Fontannaz, Guillet, Pilon, and Werlen, *A New critical study of photon production in hadronic collisions*, Phys. Rev. **D73** (2006) p. 094007, arXiv: hep-ph/0602133 [hep-ph].

[20] Eskola, Paakkinen, Paukkunen, and Salgado, *EPPS16: Nuclear parton distributions with LHC data*, Eur. Phys. J. **C77** (2017) p. 163, arXiv: 1612.05741 [hep-ph].

[21] Kovarik et al., *nCTEQ15 - Global analysis of nuclear parton distributions with uncertainties in the CTEQ framework*, Phys. Rev. **D93** (2016) p. 085037, arXiv: 1509.00792 [hep-ph].

[22] ATLAS Collaboration, *The ATLAS Experiment at the CERN Large Hadron Collider*, JINST **3** (2008) S08003.

[23] ATLAS Collaboration, *Performance of the ATLAS Trigger System in 2015*, Eur. Phys. J. C **77** (2017) p. 317, arXiv: 1611.09661 [hep-ex].

[24] ATLAS Collaboration, *Measurement of the photon identification efficiencies with the ATLAS detector using LHC Run-1 data*, Eur. Phys. J. **C76** (2016) p. 666, arXiv: 1606.01813 [hep-ex].

[25] ATLAS Collaboration, *Electron and photon energy calibration with the ATLAS detector using LHC Run 1 data*, Eur. Phys. J. C **74** (2014) p. 3071, arXiv: 1407.5063 [hep-ex].

[26] ATLAS Collaboration, *Topological cell clustering in the ATLAS calorimeters and its performance in LHC Run 1*, Eur. Phys. J. **C77** (2017) p. 490, arXiv: 1603.02934 [hep-ex].

[27] Sjostrand, Mrenna, and Skands, *A Brief Introduction to PYTHIA 8.1*, Comput. Phys. Commun. **178** (2008) p. 852, arXiv: 0710.3820 [hep-ph].

[28] Ball et al., *Parton distributions with LHC data*, Nucl. Phys. **B867** (2013) p. 244, arXiv: 1207.1303 [hep-ph].

[29] ATLAS Collaboration, *ATLAS Pythia 8 tunes to 7 TeV data*, ATL-PHYS-PUB-2014-021, 2014, URL: https://cds.cern.ch/record/1966419.

[30] Agostinelli et al., *GEANT4: A Simulation toolkit*, Nucl. Instrum. Meth. **A506** (2003) p. 250.

[31] ATLAS Collaboration, *The ATLAS Simulation Infrastructure*, Eur. Phys. J. C **70** (2010) p. 823, arXiv: 1005.4568 [physics.ins-det].

[32] Bourhis, Fontannaz, and Guillet, *Quarks and gluon fragmentation functions into photons*, Eur. Phys. J. **C2** (1998) p. 529, arXiv: hep-ph/9704447 [hep-ph].

[33] Dulat et al., *New parton distribution functions from a global analysis of quantum chromodynamics*, Phys. Rev. **D93** (2016) p. 033006, arXiv: 1506.07443 [hep-ph].

[34] Chien, Emerman, Kang, Ovanesyan, and Vitev, *Jet Quenching from QCD Evolution*, Phys. Rev. **D93** (2016) p. 074030, arXiv: 1509.02936 [hep-ph].

[35] ATLAS Collaboration, *Measurement of the inclusive isolated prompt photons cross section in pp collisions at $\sqrt{s} = 7$ TeV with the ATLAS detector using 4.6 fb^{-1}*, Phys. Rev. D **89** (2014) p. 052004, arXiv: 1311.1440 [hep-ex].

[36] ATLAS Collaboration, *High-E_{T} isolated-photon plus jets production in pp collisions at $\sqrt{s} = 8$ TeV with the ATLAS detector*, Nucl. Phys. B **918** (2017) p. 257, arXiv: 1611.06586 [hep-ex].

[37] ATLAS Collaboration, *Luminosity determination in pp collisions at $\sqrt{s} = 8$ TeV using the ATLAS detector at the LHC*, Eur. Phys. J. C **76** (2016) p. 653, arXiv: 1608.03953 [hep-ex].